Geophys. J. Int. (2005) **160,** 331–343 doi: 10.1111/j.1365-246X.2004.02461.x

Maximum horizontal stress orientations in the Cooper Basin, Australia: implications for plate-scale tectonics and local stress sources

Scott D. Reynolds,[1] Scott D. Mildren,[1,*] Richard R. Hillis,[1] Jeremy J. Meyer[2] and Thomas Flottmann[3]

[1]*Australian School of Petroleum, The University of Adelaide, SA,* 5005, *Australia. E-mail: reynolds@asp.adelaide.edu.au*
[2]*JRS Petroleum Research Pty Ltd,* PO Box 319, *Kent Town, SA,* 5071*, Australia*
[3]*Santos Ltd, Brisbane, Qld,* 4000*, Australia*

Accepted 2004 August 17. Received 2004 August 17; in original form 2003 September 9

SUMMARY

Borehole breakouts and drilling-induced tensile fractures (DITFs) were interpreted in 61 wells in the Cooper Basin indicating an average maximum horizontal stress orientation of 101°N. A total of 890 borehole breakouts and 608 DITFs were interpreted in the Cooper Basin. The approximately east–west maximum horizontal stress orientation is consistent over much of the basin, except in the Patchawarra Trough where maximum horizontal stress rotates to a northwest–southeast orientation. This rotation in maximum horizontal stress orientation is consistent with *in situ* stress data to the northwest of the Cooper Basin. The stress field in the Cooper Basin appears to mark the apex of a major horseshoe-shaped rotation in maximum horizontal stress direction across central eastern Australia. Finite element modelling of the *in situ* stress field of the Indo–Australian Plate (IAP) using a range of plate-scale tectonic forces is able to match the regional maximum horizontal stress orientation over most of Australia reasonably well, including the mean east–west maximum horizontal stress orientation in the Cooper Basin. However, plate boundary–scale modelling does not adequately match the horseshoe-shaped stress rotation across central eastern Australia. The average east–west maximum horizontal stress orientation in the Cooper Basin indicates that stresses from tensional forces acting along the Tonga–Kermadec subduction zone are not transmitted into the interior of the Australian plate. The majority of the tensional forces associated with the Tonga–Kermadec subduction zone are most likely accommodated along the numerous spreading centres within the Lau–Havre backarc basin. A number of more localized stress anomalies have also been identified. These cannot be explained by plate-scale tectonic forces and are possibly a result of geological structure and/or density contrasts locally perturbing the stress field.

Key words: Cooper Basin, plate tectonics, stress orientation.

1 INTRODUCTION

In most continental areas, the first-order maximum horizontal stress (S_{Hmax}) orientation is consistent and broadly matches the direction of absolute plate velocity (Zoback *et al.* 1989; Richardson 1992; Gölke & Coblentz 1996). Thus, the first-order intraplate stress field appears to be controlled by plate driving forces such as ridge push (Zoback *et al.* 1989; Richardson 1992). In contrast, the Australian intraplate stress field is highly variable and does not parallel the north-northeast direction of absolute plate velocity for the Indo–Australian Plate (IAP). Consequently, on initial inspection, plate driving forces do not appear to control the first-order intraplate stress field in continental Australia. However, a number of studies have shown that plate driving forces do indeed play a critical role in controlling the Australian intraplate stress field if the heterogeneous convergent northeastern boundary of the IAP is recognized (Cloetingh & Wortel 1986; Coblentz *et al.* 1995, 1998). Thus, the complex nature of the Australian stress field provides an ideal location to investigate the interaction between the intraplate stress field and plate boundary forces. In this study, we present a large number of high-quality *in situ* stress data for the Cooper Basin, which adds significantly to our understanding of the nature as well as the underlying controls of the stress field in continental Australia.

The Cooper Basin is a northeast–southwest trending intracratonic basin located in central Australia (Fig. 1). The basin is located a

*Now at: JRS Petroleum Research Pty Ltd, PO Box 319, Kent Town, SA, 5071, Australia.

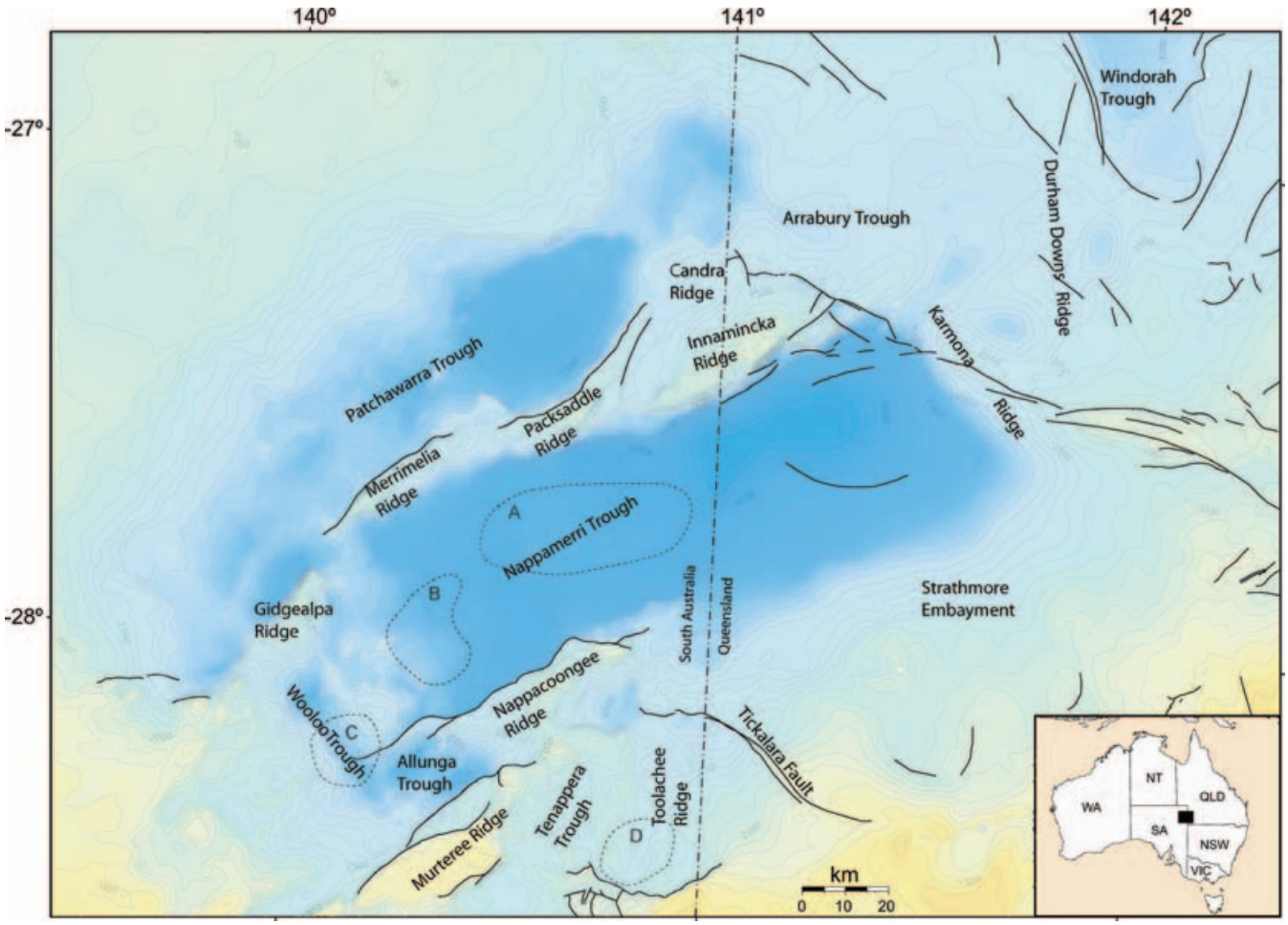

Figure 1. Location map of the Cooper Basin showing the major structural elements of the basin. Colour background image shows depth to basement with major basement-cutting faults also shown. Dashed lines indicate extent of gravity lows relating to three confirmed (A, B, C) and one inferred (D) Carboniferous granite bodies within the area of investigation.

significant distance from the nearest plate boundary and hence provides an ideal location to test the influence of plate boundary forces acting on the IAP. When combined with stress information from surrounding areas, the Cooper Basin plays a critical role in constraining the modelled stress field in central Australia. Furthermore, the S_{Hmax} orientation in the Cooper Basin is approximately perpendicular to the north-northeast direction of absolute plate velocity for the IAP.

The Cooper Basin is the largest onshore oil and gas province in Australia. Extensive drilling has occurred in the Cooper Basin since the first natural gas discovery in 1963. As a result, a substantial database of high-quality image log data exists for the Cooper Basin. Data presented in this study comes from both the South Australia and Queensland sectors of the basin and comprises a total of 42 image logs providing over 19 km of well bore image. A number of older dipmeter logs have also been included in the analysis.

The *in situ* stress data in the Cooper Basin is important to our understanding of the Australian stress field, as limited *in situ* stress data exist for central Australia. The stress data that is available indicates a range of S_{Hmax} orientations from north–south in the Amadeus and Bowen basins (Fig. 2), to a highly scattered east–west orientation in the Flinders Ranges and also a variable S_{Hmax} orientation in the Sydney Basin (Hillis *et al.* 1999; Hillis & Reynolds 2000; Fig. 2). Thus *in situ* stress data for the Cooper Basin is critical to understanding the Australian stress field. Previously published stress data has indicated an average east–west S_{Hmax} orientation in the Cooper Basin (Hillis & Reynolds 2000). However, this was only based on 14 stress measurements and, hence, did not reveal many of the stress field features uncovered by this study.

2 TECTONIC AND GEOLOGICAL SETTING

The Cooper Basin is a Late Carboniferous to Middle Triassic, non-marine sedimentary basin located in central Australia (Hill & Gravestock 1995). The focus of this study was on the South Australia and adjacent Queensland sectors of the basin. The South Australia sector of the basin contains the greatest thickness of productive Permian strata and hence the largest amount of well data (Gravestock & Jensen-Schmidt 1998). Consequently the majority of the stress data is located in the South Australia sector of the basin. A major unconformity occurs at the top of the Cooper Basin separating it from the overlying Eromanga Basin of Jurassic to Cretaceous age (Apak *et al.* 1997). Depth to the unconformity varies from 970 to 2800 m (Laws & Gravestock 1998). The Cooper Basin reaches a maximum depth of approximately 4400 m in its deepest trough (Laws & Gravestock 1998).

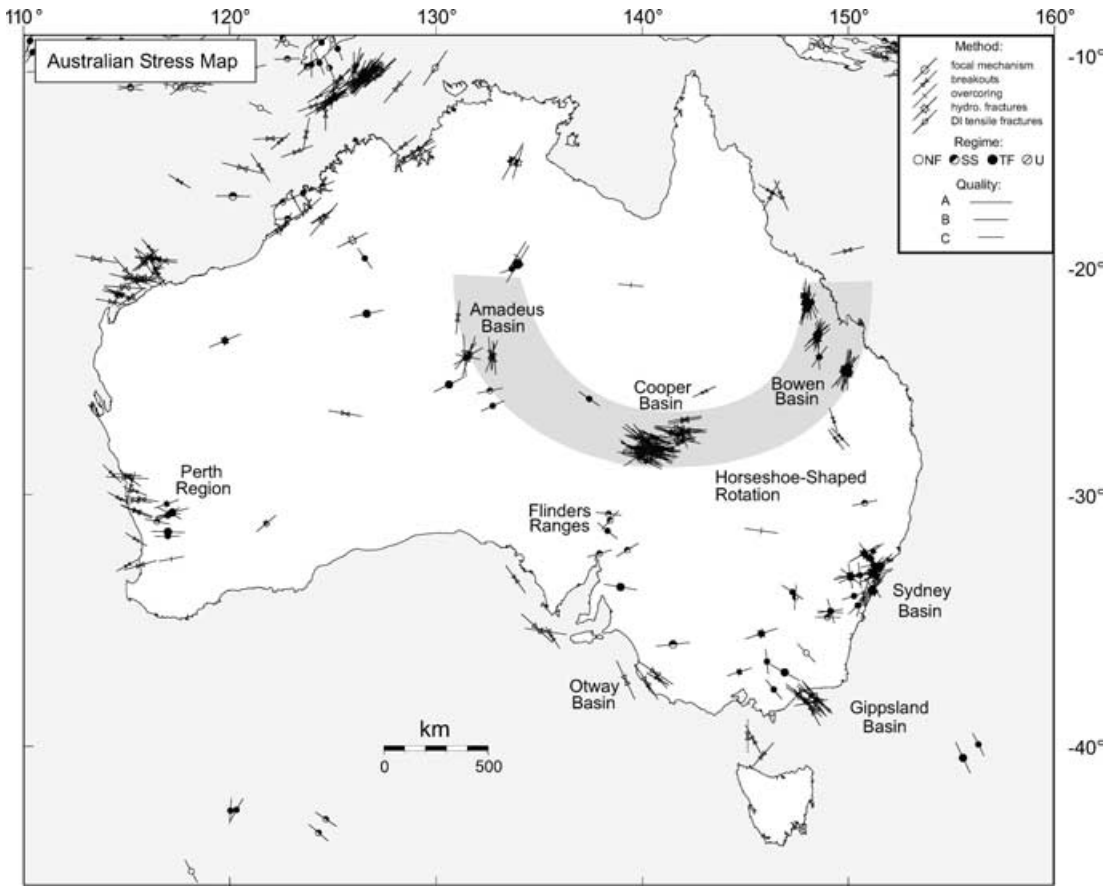

Figure 2. The Australian stress field. Maximum horizontal stress orientations are plotted for all the A–C quality data. Vector length represents the data quality. Solid, open and semi-solid stress indicator symbols represent compressional (TF), extensional (NF) and strike-slip (SS) deformation style, respectively. Grey shading indicates the horseshoe-shaped S_{Hmax} rotation across the central eastern part of the Australian continent referred to in the text. Focal mechanism = earthquake focal mechanism; breakout = borehole breakout; overcoring = overcoring measurements; hydro. fractures = hydraulic fracture measurements; geol. indicators = geological indicators; DI tensile fractures = drilling-induced tensile fractures.

In Australian terminology, overlying, successor basins are generally given different names. The Eromanga Basin is a successor basin overlying, but more widespread than, the Cooper Basin. The majority of the stress data included herein come from the Late Carboniferous to Middle Triassic Cooper Basin. However, some stress data are from the overlying Jurassic to Cretaceous Eromanga Basin, but only within the same geographic area of subcrop as the Cooper Basin. Hence, for the sake of simplicity we refer to this study as covering the Cooper Basin.

The South Australia sector of the Cooper Basin comprises a series of northeast to southwest trending ridges and troughs. The major depocentres include the Patchawarra Trough, the Nappamerri Trough and the Tennapera Trough, which are separated by two major intrabasin highs, the Gidgealpa–Merrimelia–Innamincka (GMI) Ridge and the Muteree–Nappacooongee Ridge (Fig. 1). The Nappamerri Trough extends into the Queensland sector of the basin, which also contains a number of less prominent structural features. The Arrabury–Karmona trend divides the basin into southern and northern parts, with the southern part containing most of the Permian depocentres and the northern part containing most of the Triassic depocentres (Gravestock & Jensen-Schmidt 1998). The majority of the well data used in this study is located on the intrabasin highs surrounding the major troughs. However, a few of the wells analysed are located in the Patchawarra and Nappamerri troughs.

3 BOREHOLE BREAKOUT AND DRILLING-INDUCED TENSILE FRACTURE ANALYSIS

Borehole breakouts and drilling-induced tensile fractures (DITFs) have been interpreted from both image and dipmeter log data to determine the *in situ* stress field for the Cooper Basin. Borehole breakouts form when the circumferential stress acting around a well bore exceeds the compressive strength of the rock (Bell & Gough 1979; Zoback *et al.* 1985; Fig. 3). When this arises in a vertical well, conjugate shear fractures form at the well bore wall centred on the minimum horizontal stress (S_{hmin}) direction, causing the rock to spall off (Gough & Bell 1982). As a consequence, the well bore becomes enlarged in the S_{hmin} direction (Fig. 3).

Borehole breakouts can be interpreted using either dipmeter or imaging tools. The high-resolution dipmeter tool (HDT) was commonly used in older wells and has now been largely replaced by imaging tools. A number of wells with dipmeter logs have been included in this study, however the majority of the analysis in this study has been conducted on wells with image log data from Schlumberger's Formation Microscanner (FMS) tool. The FMS tool consists of four pads with 16 buttons on each pad that measure microresistivity variations of the rock surrounding the borehole. Schlumberger's newer image tool, the Formation Microimager (FMI), has been run in a small number of wells on the Queensland sector of the basin.

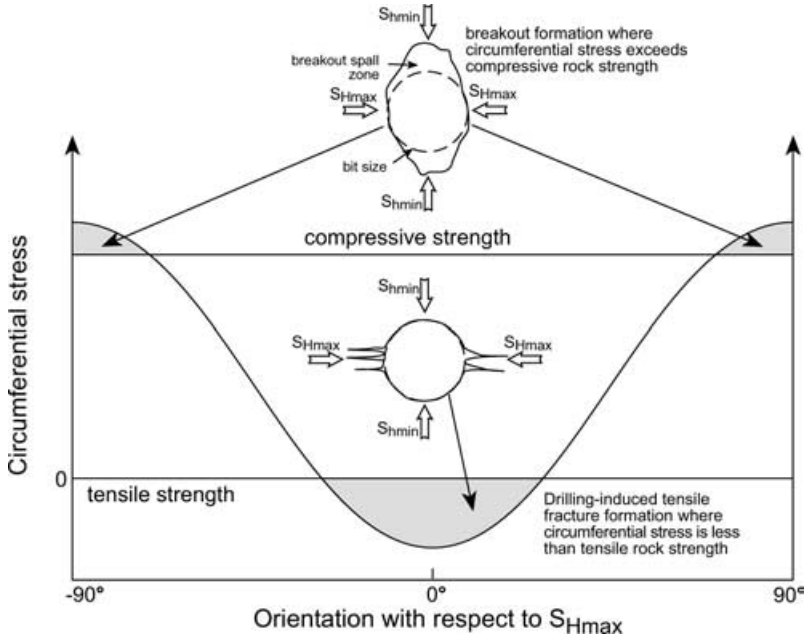

Figure 3. Circumferential stress around a vertical well bore with respect to the S_{Hmax} orientation. Breakout formation occurs where the circumferential stress exceeds the compressive rock strength. Drilling-induced tensile fracture (DITF) formation occurs at 90° to the breakouts where the circumferential stress is less than the tensile rock strength.

The FMI tool consists of four pads and four flaps each with 24 buttons providing significantly increased well bore coverage. Borehole breakouts on image logs are generally poorly resolved (poor pad-wall contact), blobby zones of low resistivity where drilling mud has invaded breakout-related fractures (Fig. 4).

DITFs form in the orientation of S_{Hmax} when the circumferential stress around the well bore is less than the tensile strength of the rock (Brudy & Zoback 1999; Fig. 3). Their formation is analogous to fracture initiation during a hydraulic fracture test and is the result of the natural stress state being perturbed by drilling. However, DITFs do not propagate into the well bore wall unless the well bore fluid pressure exceeds the minimum principal stress (Barton *et al.* 1998). Hence no lost mud is recorded. DITFs can form under a wide range of stress conditions and do not necessarily require significant well bore fluid pressures (Peska & Zoback 1995). The DITFs are dark in colour (high conductivity) as they are filled by drilling mud. They generally have well-defined edges (Fig. 4). In contrast, cemented natural fractures tend to be resistive. DITFs can only be recognized on image logs (Fig. 4).

A magnetic declination correction of between 7° and 8° east had previously been applied to all logs prior to interpretation. Each well containing borehole breakouts was ranked using the World Stress Map (WSM) scheme (Zoback 1992). The wells containing DITFs were ranked using the same criteria set out in the WSM scheme for borehole breakouts, because no formal criteria for ranking DITFs exists.

4 STRESS ORIENTATIONS IN THE COOPER BASIN AND SURROUNDING AREAS

A total of 890 borehole breakouts and 608 DITFs have been interpreted from 61 wells in the Cooper Basin (Tables 1 and 2). Borehole breakouts were interpreted in 57 wells while 27 wells were interpreted to contain DITFs. Only wells ranked A to C quality on the WSM ranking scheme were considered to have a statistically significant average S_{Hmax} orientation. Thus, D-quality wells were not included in the statistical analysis and were not plotted on Fig. 5. Nevertheless, D-quality wells are listed in Tables 1 and 2 in order to provide a record of all wells analysed as part of this study. The mean of the mean S_{Hmax} orientations in the 47 wells with A–C quality borehole breakouts is 100°N (Table 3). The mean of the mean S_{Hmax} orientations in the 17 wells with A–C quality DITFs is 104°N (Table 3). The mean S_{Hmax} orientation from all wells with A–C quality borehole breakouts and DITFs is 101°N (Table 3). Overall the variation of the average S_{Hmax} orientation inferred from different stress indicator types and qualities is very small.

On average, the stress data for the Cooper Basin indicate an approximately east–west S_{Hmax} orientation. However, a number of geographic/geological domains have their own distinct stress trends. Stress data from four wells in the Patchawarra Trough indicate a southeast–northwest S_{Hmax} orientation (Fig. 5). Wells northeast of Gigealpa-47 on the GMI ridge exhibit a west-northwest to east-southeast S_{Hmax} orientation. In the Nappamerri Trough the stress data indicate an east–west S_{Hmax} orientation. This systematic rotation is shown more clearly on the stress trajectory map of the region (Fig. 6). The stress trajectory map indicates the averaged S_{Hmax} orientation at a given location. The stress trajectories have been calculated in order to highlight the regional trend and thus smooth any local variations such as that seen in Cowan-3. Consequently, all A to D quality stress data were included in the stress trajectory calculations and were weighted accordingly (i.e. A-quality = 4, B-quality = 3, C-quality = 2, D-quality = 1). A detailed description of the stress trajectory technique can be found in Hansen & Mount (1990). The southeast–northwest S_{Hmax} orientation in the Patchawarra Trough is also observed in Malgoona-3 located on the western edge of the basin. However, the stress trajectories do not match this rotation as closely as in the Patchawarra Trough, because there is only one stress indicator at this particular location.

Examination of the data surrounding the Cooper Basin suggests that the clockwise rotation of the S_{Hmax} orientation from the

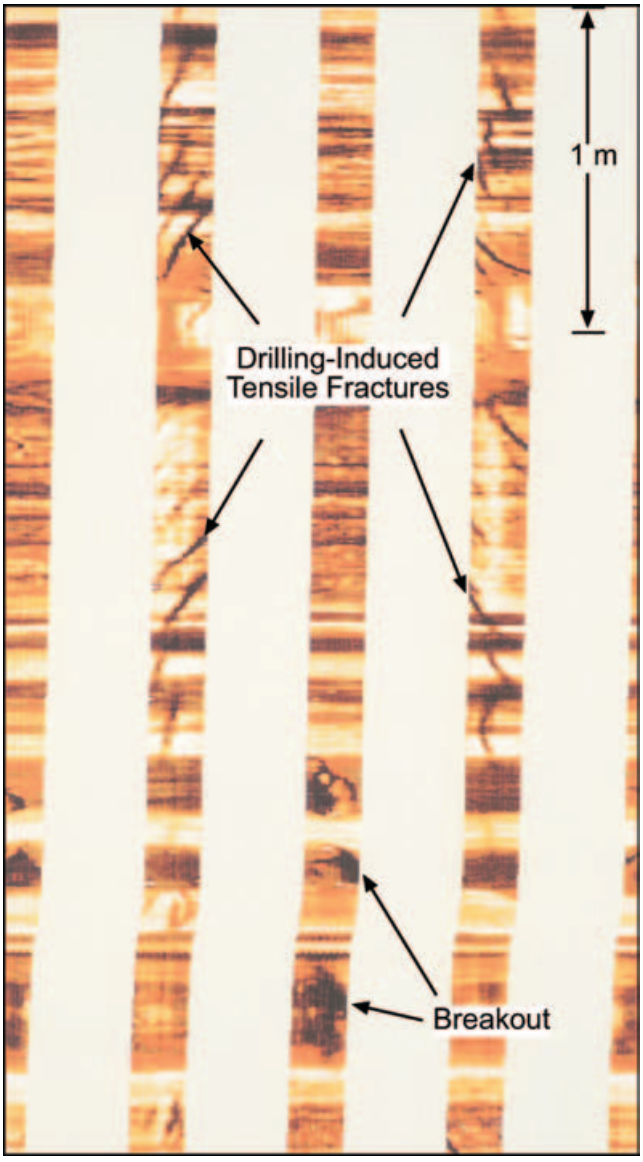

Figure 4. Bulyeroo-1 Formation Microscanner (FMS) log with borehole breakouts and drilling-induced tensile fractures (DITFs).

Nappamerri Trough to the Patchawarra Trough is part of a larger scale rotation across the Australian continent. The Amadeus Basin to the northwest of the Cooper Basin shows a north–south S_{Hmax} orientation (Fig. 2). This orientation has been determined from borehole breakouts in a number of petroleum wells and is approximately perpendicular to that obtained from the stress orientation determined in the Cooper Basin. The S_{Hmax} orientation in the Amadeus Basin is consistent with that determined from the Tennant Creek earthquake to the north (Fig. 2). Two earthquake focal mechanisms occur between the Cooper and Amadeus Basins, which indicate an approximately northwest to southeast S_{Hmax} orientation. One of the earthquake focal mechanisms is C-quality and is displayed in Fig. 2. The other earthquake focal mechanism is D-quality, but indicates a consistent S_{Hmax} orientation with the other earthquake focal mechanism, despite its poorer quality. Both stress indicators are consistent with the systematic rotation of the S_{Hmax} orientation observed in the Cooper Basin. Thus, the stress data in central Australia suggest that a major counter-clockwise rotation occurs from a north–south S_{Hmax} orientation in the Amadeus Basin to an east–west S_{Hmax} orientation in parts of the Cooper Basin.

Northeast of the Cooper Basin, the S_{Hmax} orientation is approximately north-northwest to south-southeast in the Bowen Basin (Fig. 2). The stress orientation in the Bowen Basin has been determined from engineering type (overcoring and hydraulic fracturing) *in situ* stress measurements. The engineering *in situ* stress data are particularly deep in terms of normal engineering data, going to a depth of 1 km, and are also very consistent when averaged over the entire basin (Hillis *et al.* 1999). The consistency of the stress orientation over a distance of 500 km in the Bowen Basin has led to the suggestion that this is a first-order stress trend (Hillis *et al.* 1999). Thus, the east–west S_{Hmax} orientation in the eastern Cooper Basin appears to also rotate to an approximately north–south orientation in the Bowen Basin. Both Ramses-1 and Coonaberry-1, located in the northeastern corner of the study area, show a slight rotation to an east-northeast to west-southwest S_{Hmax} orientation. However, the S_{Hmax} orientation in the two wells only differs by approximately 10° from the S_{Hmax} orientation in other nearby wells and, hence, is not as well defined as the rotation on the western side of the basin. A pre-existing borehole breakout to the northeast of the study area shows a significantly greater rotation than either Ramses-1 or Coonaberry-1 (Fig. 2). Consequently we feel the S_{Hmax} orientations in Ramses-1 and Coonaberry-1 indicate the start of the large-scale rotation of the stress field from east–west in the central Cooper Basin to the north–south S_{Hmax} orientation observed in the Bowen Basin. Nonetheless, further stress data are required on the eastern side of the basin to confirm the extent and nature of the stress rotation. Thus, the stress field in the Cooper Basin appears to mark the apex of a horseshoe-shaped rotation in the S_{Hmax} direction across central eastern Australia. Furthermore, the mean S_{Hmax} orientation (101°N) for the Cooper Basin is perpendicular to the direction of absolute plate velocity.

The Flinders Ranges, directly south of the Cooper Basin, is characterized by a mean S_{Hmax} orientation of 088°N (Hillis & Reynolds 2000; Fig. 2). The Flinders Ranges is one of the most seismically active areas in Australia and, as a consequence, all of the stress indicators in the Flinders Ranges are from earthquake focal mechanism. The stress field in the Flinders Ranges is particularly scattered, which is probably the result of earthquakes occurring along pre-existing planes of weakness. Despite the scattered *in situ* stress measurements, the regional stress field in the Flinders Ranges appears to be consistent with that of the Cooper Basin. An east–west S_{Hmax} orientation has also been recorded for the Perth region, located in southwestern Australia (Reynolds & Hillis 2000; Fig. 2). Hence the southern section of Australia, which includes the Perth region, Flinders Ranges and Cooper Basin, is characterized by a broadly east–west S_{Hmax} orientation.

In southeastern Australia the stress field rotates from the east–west in the Cooper Basin and Flinders Ranges to a southeast–northwest S_{Hmax} orientation in the Otway and Gippsland basins (Fig. 2). The S_{Hmax} orientations in the Otway and Gippsland basins are both consistent and are thought to represent first-order stress trends (Hillis & Reynolds 2000). East of the Cooper Basin, the Sydney Basin has a particularly scattered stress trend and is thought to display the influence of local sources of stress rather than large-scale tectonic sources (Hillis *et al.* 1999).

5 IMPLICATIONS FOR PLATE BOUNDARY FORCES

The Australian intraplate stress field provides a unique opportunity to investigate the forces acting along the boundaries of the

Table 1. List of wells containing borehole breakouts. Depth and lengths are in metres. Azi = circular mean azimuth of S_{Hmax}; SD = circular standard deviation; Q = quality.

Well	Location		Log	No.	Depth		Unweighted			Length weighted			
	Lat.	Long.			Top	Bot	Azi	SD	Q	∑ L	Azi	SD	Q
Bartilla-1	−28.252	139.878	FMS	9	2024	2183	091	9	B	2.6	091	9	B
Baryulah-3	−27.745	141.844	HDT	17	1951	2560	075	20	B	79	—	—	—
Biala-7	−28.536	140.369	FMS	2	1237	1243	104	5	C	1	104	5	C
Big Lake-54	−28.224	140.341	FMS	56	2374	3253	108	12	A	200	111	11	A
Brolga-3	−27.584	140.008	FMS	45	2689	2988	129	6	A	110	130	5	A
Bulyeroo-1	−27.839	140.577	FMS	14	2716	2920	081	7	A	—	—	—	—
Caladan-1	−28.218	139.924	FMS	14	1949	2027	121	9	A	3.6	123	10	A
Challum-9	−27.395	141.588	FMS	11	1522	2346	108	7	A	—	—	—	—
Challum-10	−27.409	141.610	FMS	15	1909	2609	113	8	A	—	—	—	—
Challum-12	−27.427	141.649	FMS	33	1927	2675	106	7	A	—	—	—	—
Coonaberry-1	−26.851	142.104	HDT	24	2226	2749	080	18	B	81	—	—	—
Daralingie-10	−28.361	139.974	HDT	2	1926	1942	040	18	D	8	130	18	D
Dirkala South-1	−28.527	140.043	FMS	16	1305	2131	107	3	A	7.6	106	2	A
Dorodillo-1	−28.157	139.976	FMS	21	2287	2547	114	10	A	10.3	113	9	A
Dorodillo-3	−28.129	139.958	FMS	3	2519	2583	101	4	D	0.3	102	4	D
Dullingari-10	−28.055	140.886	HDT	2	1613	1624	121	0	D	5.6	121	0	D
Dullingari-11	−28.053	140.858	HDT	2	1629	1668	116	3	D	13	114	2	D
Dullingari-13	−28.106	140.875	HDT	5	1249	1519	072	24	C	16	076	18	C
Dullingari-24	−28.111	140.893	HDT	5	—	—	087	14	C	12	088	15	C
Dullingari-27	−28.115	140.875	HDT	20	729	1423	098	18	B	65	100	19	B
Dullingari-33	−28.083	140.854	HDT	3	—	—	081	50	E	6	083	41	E
Dullingari-47	−28.11	140.89	FMS	3	1498	1570	099	8	D	9	097	7	D
Dullingari North-8	−28.088	140.858	FMS	32	2150	2839	097	7	A	396	098	6	A
Fly Lake-8	−27.653	139.936	FMS	38	2668	2950	126	8	A	37.7	126	7	A
Gidgealpa-54	−28.033	139.994	FMS	5	2224	2241	092	5	C	3.2	090	4	C
Jena-12	−28.503	140.312	FMS	1	1279	1280	093	0	D	0.5	093	0	D
Juno North-1	−27.650	141.852	FMI	13	2201	2804	103	3	A	518	101	2	A
Kananda-1	−27.152	141.821	HDT	42	2609	2804	095	8	A	137	—	—	—
Katingawa-1	−28.185	140.792	FMS	42	2224	2952	104	14	B	115	105	11	A
Koree South-1	−28.453	139.966	FMS	3	2184	2252	153	9	D	1	150	7	D
Lepena-2	−28.204	140.688	FMS	24	1920	2226	108	8	A	12.4	106	12	A
Merrimelia-30	−27.728	140.185	FMS	14	1873	2168	108	6	A	19	108	6	A
Merrimelia-32	−27.736	140.178	FMS	6	1675	2090	115	5	B	21	114	3	B
Moomba-73	−28.018	140.256	FMS	29	2497	2994	094	6	A	66	093	5	A
Moomba-74	−28.04	140.128	FMS	7	2485	2561	099	3	B	14	097	3	B
Moomba-78	−28.074	140.323	FMS	21	2500	2665	093	6	A	—	—	—	—
Moorari-7	−27.57	140.136	HDT	6	1907	2403	142	11	B	17	144	12	B
Mudlalee-3	−28.301	140.546	FMS	22	1157	1640	108	6	A	39.4	112	9	A
Munkah-7	−27.434	141.897	FMI	—	2073	2377	100	—	C	143	—	—	—
Nappacoongee-2	−28.027	140.778	HDT	12	1453	1906	089	17	B	98	092	15	B
Nappacoongee East-1	−28.026	140.781	FMS	11	1745	1958	097	7	A	—	—	—	—
Pondrinie-9	−27.563	140.651	FMS	17	1871	2286	110	11	B	—	—	—	—
Ramses-1	−26.764	142.102	HDT	55	1993	2896	082	18	B	168	—	—	—
Roti-2	−27.383	142.180	HDT	8	2164	2393	081	8	B	20	—	—	—
Roti West-1	−27.367	142.143	HDT	37	853	2377	089	10	A	127	—	—	—
Stokes-5st	−28.342	141.041	FMI	—	1890	2469	090	—	C	73	—	—	—
Swan Lake-4	−27.852	140.126	FMS	23	2513	3087	116	7	A	161	117	6	A
Wackett-10	−27.512	141.990	FMI	—	1615	1951	157	—	C	107	—	—	—
Wackett SE-1	−27.595	142.007	HDT	6	1097	2560	123	42	E	10	—	—	—
Wantana-1	−27.633	140.423	HDT	8	2500	2751	100	8	B	21	100	8	B
Wilpinnie-1	−28.059	140.735	HDT	11	1357	2149	083	16	B	245	079	22	C
Wilpinnie-2	−28.048	140.764	HDT	8	2081	2268	106	13	B	17.2	110	15	B
Winninia North-1	−27.814	141.888	FMI	—	2091	2390	060	—	C	134	—	—	—
Wippo East-1	−27.294	142.121	HDT	11	1926	2478	086	7	B	38	—	—	—
Wippo East-2	−27.269	142.131	HDT	26	884	1859	089	12	A	338	—	—	—
Woolkina-1	−27.59	140.117	HDT	1	—	—	152	—	D	4	152	—	D
Yalchirrie-1	−27.543	140.578	FMS	29	2291	2585	116	15	B	11	104	35	D

IAP (Fig. 7). The Cooper Basin is centrally located on the Australian continent and thus provides an ideal location to investigate the force balance along the plate boundaries surrounding the IAP. Recent finite element modelling of the IAP has used a new basis-set approach, which searches over a wide range of plate boundary combinations and calculates the misfit between the modelled and the observed stress fields (Reynolds *et al.* 2002). An observed regional stress field based on observations in 12 stress provinces provided

Table 2. List of wells containing DITFs. Depth and lengths are in metres. Azi = circular mean azimuth of S_{Hmax}; SD = circular standard deviation; Q = quality.

Well	Location		Log	No.	Depth		Unweighted		
	Lat.	Long.			Top	Bot	Azi	SD	Q
Barina-1	−28.301	139.917	FMS	6	1989	2006	108	3	B
Bartilla-1	−28.252	139.878	FMS	85	2051	2169	093	11	A
Big Lake-54	−28.224	140.341	FMS	22	2376	3249	109	6	A
Brolga-3	−27.584	140.008	FMS	5	2724	2905	134	11	C
Bulyeroo-1	−27.839	140.577	FMS	32	2716	2920	089	20	B
Caladan-1	−28.218	139.924	FMS	17	1966	2036	120	6	A
Cowan-3	−28.317	140.043	FMS	21	2379	2448	063	6	A
Dirkala South-1	−28.527	140.043	FMS	21	1801	2059	114	5	A
Dorodillo-1	−28.157	139.976	FMS	2	2266	2285	123	0	D
Dorodillo-3	−28.129	139.958	FMS	3	2534	2637	102	11	D
Dullingari-47	−28.110	140.89	FMS	54	1459	1530	096	8	A
Dullingari North-8	−28.088	140.858	FMS	58	2134	2816	093	8	A
Farina-2	−28.290	139.922	FMS	2	2020	2021	102	1	D
Fly Lake-8	−27.653	139.936	FMS	2	2891	2919	122	7	D
Gidgealpa-55	−28.038	140.001	FMS	2	1238	1398	099	1	D
Jena-12	−28.503	140.312	FMS	1	1233	1234	084	0	D
Malgoona-3	−28.129	139.619	FMS	9	1994	2097	129	13	B
Merrimelia-30	−27.728	140.185	FMS	12	2224	2272	103	30	D
Merrimelia-32	−27.736	140.178	FMS	2	2195	2196	095	5	D
Moomba-73	−28.018	140.256	FMS	14	2860	2949	093	13	B
Moomba-78	−28.074	140.323	FMS	64	2535	2978	097	16	B
Mudlalee-3	−28.301	140.546	FMS	25	1460	1634	114	11	A
Nappacoongee East-1	−28.026	140.781	FMS	136	1745	1958	094	15	B
Narcoonowie-4	−28.490	140.715	FMS	2	1579	1581	092	4	D
Pondrinie-9	−27.563	140.651	FMS	4	1871	2286	094	11	C
Wooloo South-1	−28.285	140.040	FMS	2	2516	2521	106	3	D
Yalchirrie-1	−27.543	140.578	FMS	5	2566	2582	121	3	C

constraint for the modelling (Reynolds *et al.* 2002). The new modelling has demonstrated that the regional stress field in continental Australia can be accounted for by a combination of the principal tectonic forces acting on the plate (Reynolds *et al.* 2002).

Regional stress orientations in the western half of the Australian continent can be accounted for by combining a ridge push force along with a compressional force on the Himalayan and New Guinea boundaries (Coblentz *et al.* 1995, 1998). Application of these forces on the IAP causes the stress field to be focused orthogonal to the Himalayan and New Guinea boundaries with the stress field rotating between the two boundaries. Hence, an east–west S_{Hmax} orientation is produced in the Perth and Carnarvon basins rotating to northeast–southwest in the Canning and Bonaparte basins and north–south in the Amadeus Basin. Modelling the observed regional stress field in the eastern half of Australia required compressional forces along the Solomon, New Hebrides, Tonga–Kermadec, New Zealand and south of New Zealand plate boundaries (Reynolds *et al.* 2002).

Recent modelling has shown that the mean east–west S_{Hmax} orientation in the Cooper Basin, along with the entire regional stress field of Australia, can be reasonably well modelled using a combination of plate boundary forces (Reynolds *et al.* 2002; Fig. 8). However, the plate-scale tectonic modelling does not fully predict the horseshoe-shaped stress rotation in central eastern Australia shown in Fig. 2. In order to fit the observed stress field in the Cooper Basin, the modelled S_{Hmax} orientation in the Amadeus Basin is rotated in a more easterly direction than the observed S_{Hmax} orientation. Furthermore, in the region between the Cooper and Amadeus basins the stress orientation predicted by the modelling is approximately perpendicular to the orientation observed from the two earthquake focal mechanisms. A regional stress source, as compared to plate-scale sources of stress used in the modelling described herein, is required in order to account for the horseshoe-shaped rotation of the stress field between the Amadeus, Cooper and Bowen basins. A possible regional source of stress is the rheology variations between different geological provinces. Rheology variations are not currently included in the tectonic force modelling undertaken in this study. However, recent models of the stress field of the IAP incorporating such rheological variations by Dyksterhuis & Müller (2004) provide a poorer match to the observed stress data in this area. Thus, current modelling cannot fully match the horseshoe-shaped rotation in central eastern Australia using either plate-scale or regional sources of stress.

Results from the modelling indicate that the mean east–west S_{Hmax} orientation in the Cooper Basin can be modelled using a range of plate boundary force combinations. Thus, no single plate boundary alone controls the stress orientation in the Cooper Basin. The east–west S_{Hmax} orientation can be achieved in the Cooper Basin by balancing the forces acting on the northeast and southeast boundaries of the plate. The Tonga–Kermadec subduction zone, directly to the east of Australia, significantly influences the Cooper Basin stress field (Fig. 7). Large compressional forces applied at the Tonga–Kermadec boundary produce an east–west S_{Hmax} in the Cooper Basin, however this also creates a large misfit between the observed and modelled stress field in other areas of eastern Australia, such as the Bowen Basin. Large tensional forces applied at the Tonga–Kermadec boundary, as modelled by Cloetingh & Wortel (1986), result in a north–south S_{Hmax} orientation in the Cooper Basin and also over most of eastern Australia. Moderate compressional forces along the Tonga–Kermadec subduction zone result in the best fit to the observed stress field in the Cooper Basin. Moderate tensional forces along the Tonga–Kermadec subduction zone can fit the

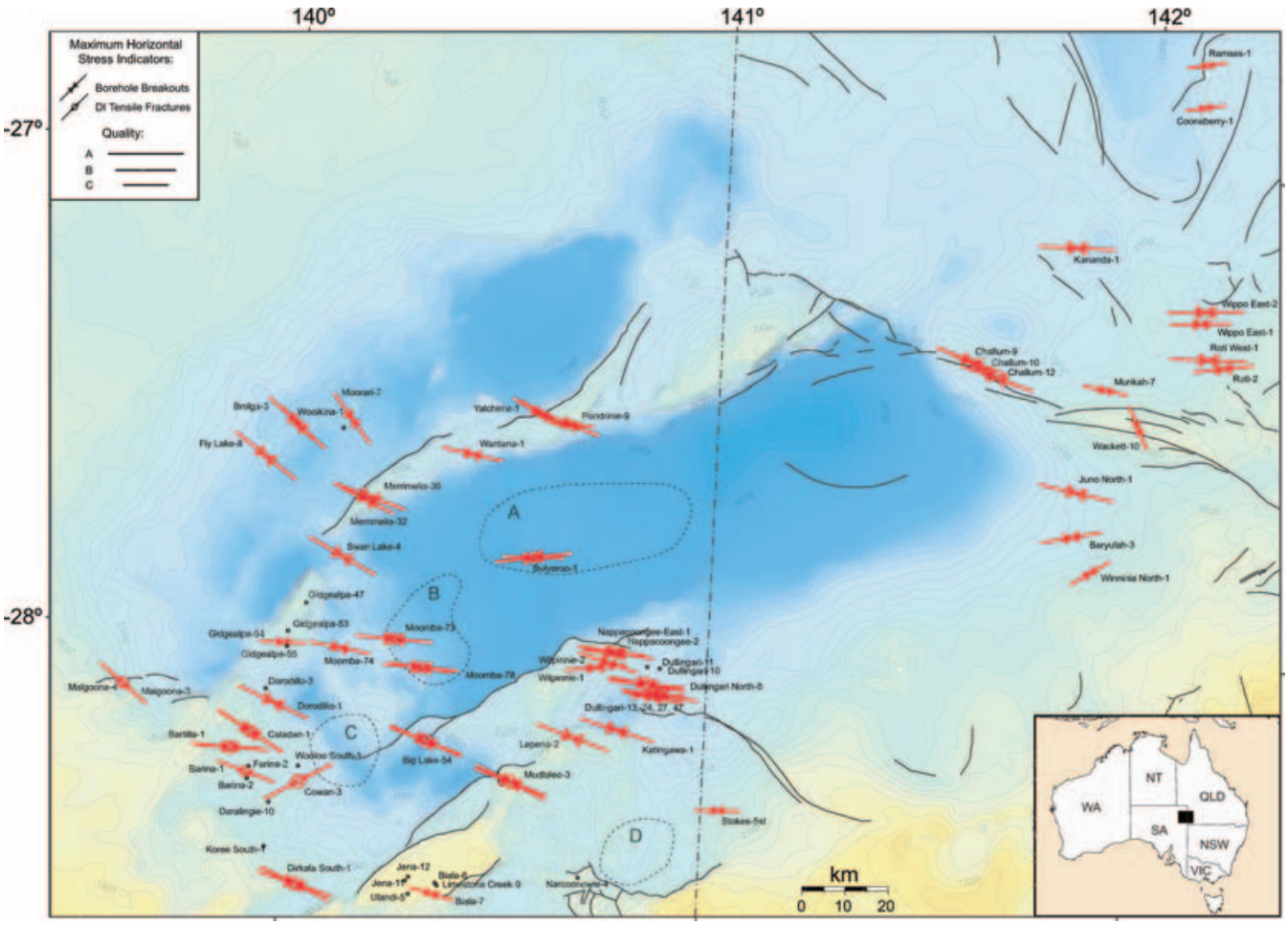

Figure 5. Maximum horizontal stress orientations (A–C quality) combined with depth to basement map and major basement cutting faults for the Cooper Basin.

Table 3. Summary of well average S_{Hmax} azimuth for the Cooper Basin.

Indicator type	Quality	Number	Azimuth	Standard deviation
Breakout	A–C	47	100°N	17°
DITF	A–C	17	104°N	17°
Breakout + DITF	A–C	64	101°N	19°

observed stress field in the Cooper Basin. However, this results in a poorer fit between the modelled and observed stress fields in the rest of Australia, particularly throughout Western Australia.

The IAP is overriding the Pacific Plate along the Tonga–Kermadec subduction zone, with backarc spreading occurring on the IAP side. This suggests the existence of tensional forces related to the Tonga–Kermadec subduction zone. However, the *in situ* stress data in eastern and central Australia indicate a reverse fault stress regime, which is incompatible with large tensional forces at the Tonga–Kermadec subduction zone. Hence, we conclude that tensional forces associated with backarc spreading are not transmitted into the plate interior. We propose that the majority of the tensional forces associated with the Tonga–Kermadec subduction zone are accommodated along the numerous spreading centres within the Lau–Havre backarc basin. Furthermore, the use of a single tectonic plate to model the Australian stress field is an oversimplification, particularly in the Lau–Havre trough, which was recently subdivided into three additional plates, the Tonga Plate, the Kermadec Plate and the Niuafo'ou Plate (Zellmer & Taylor 2001; Bird 2003).

When the modelled stress field is constrained to the Australian regional stress field without using the mean east–west S_{Hmax} orientation in the Cooper Basin, a north–south S_{Hmax} orientation is predicted for most of central and eastern Australia (Fig. 9). This stress field is incompatible with the majority of scattered *in situ* stress data throughout southeastern Australia, which indicate S_{Hmax} orientations between east–west and southeast–northwest (Fig. 2). However, the scattered stress data are not used to constrain the modelling. Hence, the average east–west S_{Hmax} orientation in the Cooper Basin also improves the fit between the modelled and observed stress fields over much of southeastern Australia.

Throughout most of the best-fitting models the stress field in the Cooper Basin and the surrounding region is relatively isotropic ($S_{\mathrm{Hmax}} = S_{\mathrm{hmin}}$) in comparison with the rest of Australia (Fig. 8). However, the relatively consistent east–west S_{Hmax} orientation determined from the observed stress data indicates that the stress field in the Cooper Basin is particularly anisotropic (i.e. $S_{\mathrm{Hmax}} \gg S_{\mathrm{hmin}}$). The co-occurrence of both borehole breakouts and DITFs in many Cooper Basin wells confirms this stress anisotropy. This discrepancy between the magnitude of the observed and modelled stress fields also indicates the Cooper Basin may be influenced by a regional source of stress not included in the plate-scale modelling.

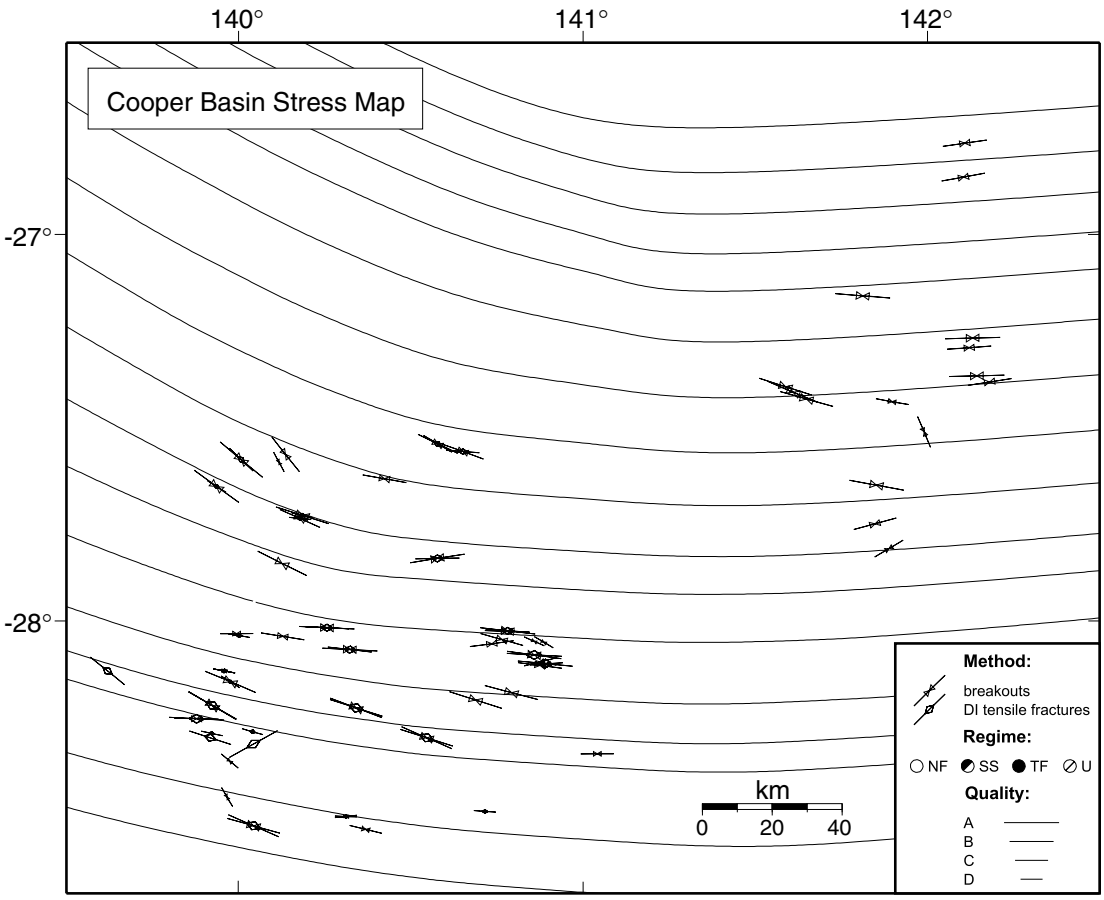

Figure 6. Stress trajectory map of the Cooper Basin. The stress trajectory map indicates the orientation of S_{Hmax} at a given location.

6 LOCAL SOURCES OF STRESS IN THE COOPER BASIN

While the observed stress orientations in the Cooper Basin are reasonably consistent, a number of smaller-scale stress perturbations cannot be accounted for by modelling using either large-scale tectonic forces or regional sources of stress. These local features include variable stress orientations in isolated wells that differ significantly from the regional stress orientation in a particular area (e.g. Cowan-3 and Challum-9, 10 and 12). Identifying the source of local stress variations (orientations and magnitudes) is often problematic as a result of the poor resolution in the stress/structural data sets and the number of effects that may be superimposed.

Local stress perturbations are the consequence of structure and/or the lateral variations in the elastic properties of rocks (Bell 1996). Numerous studies have explained perturbations in the regional stress field resulting from the presence of geological structures (e.g. Aleksandroski *et al.* 1992; Yale *et al.* 1994; Dart *et al.* 1995) and crustal density heterogeneities (e.g. Mareschal & Kuang 1986; Assameur & Mareschal 1995; Mandal *et al.* 1997). Variation in the elastic properties of the rocks can affect the stress field in two ways. If a body of rock is relatively harder than the surrounding rock then the S_{Hmax} orientation intersects the interface at right angles (Bell 1996). Alternatively, if a body of rock is relatively softer than the surrounding rock then the S_{Hmax} orientation parallels the interface (Bell 1996). The degree to which the stress field is perturbed relates to the contrast in geomechanical properties at the interface (Zhang *et al.* 1994). Stress perturbations also occur as a result of slip on pre-existing faults in rocks with homogenous elastic properties. In this situation, the stress perturbations are greatest at the tips of the discontinuity and can vary as a result of factors such as the differential stress magnitude, the friction coefficient on the discontinuity and the strike of the discontinuity relative to the far-field stress (Homberg *et al.* 1997).

The S_{Hmax} orientations interpreted from the three Challum wells are the only stress perturbation that can be confidently linked to a geological structure in the basin. All three wells show a consistent S_{Hmax} orientation that parallels a nearby basement fault (Fig. 5). The S_{Hmax} orientation determined for the three wells is rotated 20°–30° in a clockwise direction compared to the S_{Hmax} orientation in the nearest wells to the east. Fault parallel stress orientations have been observed in a number of studies (Aleksandroski *et al.* 1992; Yale *et al.* 1994). The stress rotation observed in the Challum wells is the same as that predicted by 2-D distinct element modelling of a discontinuity previously conducted by Homberg *et al.* (2004) and Homberg *et al.* (1997). The 2-D modelling shows the orientation of the local stress perturbation closely parallels the fault orientation along the mid-section of the fault in situations where there is a small angle between the S_{Hmax} orientation and the fault (Homberg *et al.* 1997; Fig. 10). Also, a high differential stress is required in order to match the fault parallel stress perturbations (Homberg *et al.* 1997), consistent with observations in the Cooper Basin. The maximum stress perturbation is modelled to occur at the extensional zones (Homberg *et al.* 1997), which are located on the southern side of the

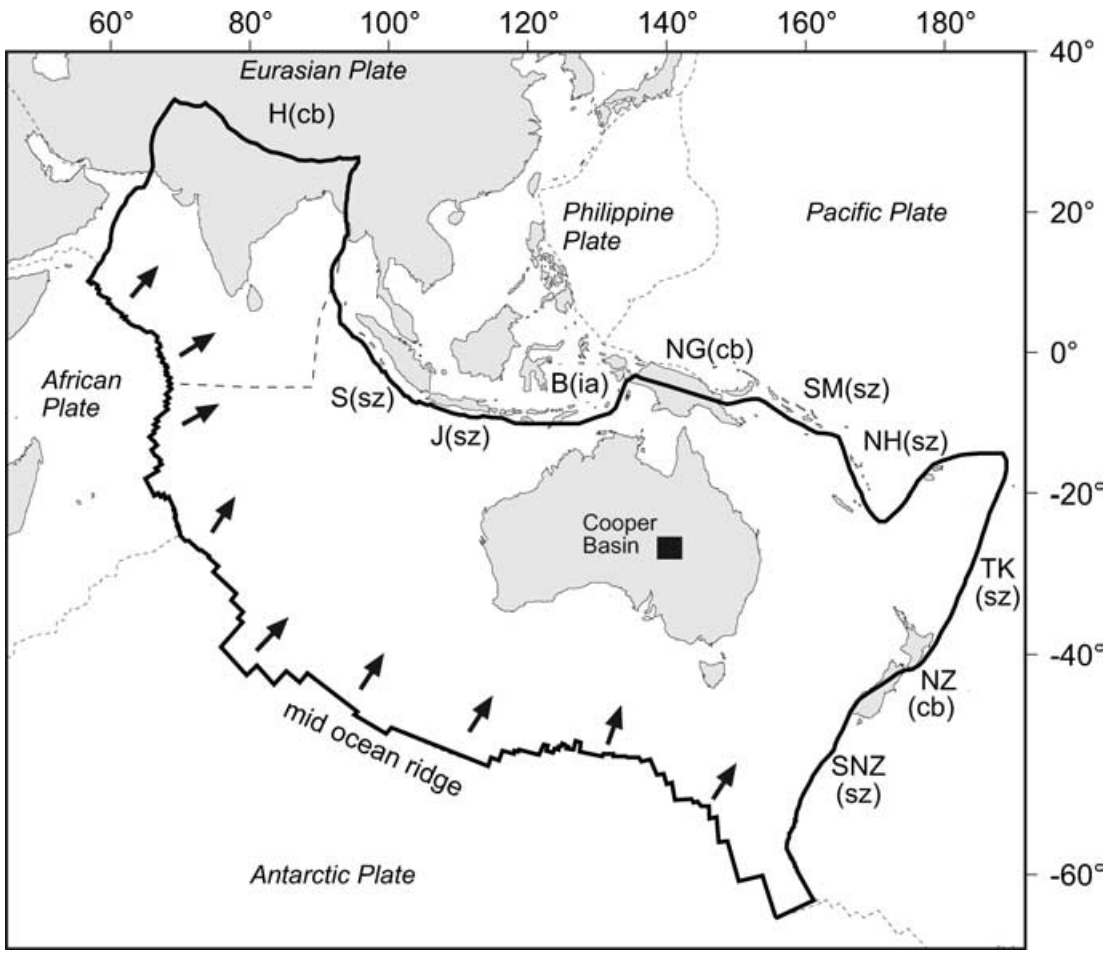

Figure 7. Indo–Australian Plate (IAP) with the boundaries used to model the *in situ* stress field of continental Australia. The large solid-filled arrows represent the force associated with ridge push. H = Himalaya; S = Sumatra Trench; J = Java Trench; B = Banda Arc; NG = New Guinea; SM = Solomon Trench; NH = New Hebrides Trench; TK = Tonga–Kermadec Trench; NZ = New Zealand; SNZ = south of New Zealand; cb = collisional boundary; sz = subduction zone; ia = island arc.

western tip of the fault and the northern side for the eastern tip of the fault for the example presented in this study (Fig. 10). However, no stress data exists at either tip of the fault to verify if this is the case.

Another major stress perturbation is observed in Cowan-3, located in the southeast corner of the basin. A large number of consistently oriented DITFs are present in Cowan-3 indicating a 063°N S_{Hmax} orientation. In comparison, the Barina-1 well, which is approximately 12 km to the west, has consistently oriented DITFs indicating a 108°N S_{Hmax} orientation. The available structural data indicate no major basement-cutting faults close to Cowan-3 (Fig. 5). Cowan-3 is however, located near one of three large Carboniferous granite bodies that have been intersected in more than 23 wells in the Nappamerri Trough (Gatehouse *et al.* 1995; Fig. 1). The granite bodies are characterized by a pronounced negative Bouguer gravity anomaly. Other granite bodies are assumed to exist within the basin on the basis of the gravity signature, however they are too deep to be reached by drilling (Fig. 1). The S_{Hmax} orientation at Cowan-3 rotates perpendicular to the granite body, oblique to adjacent wells and is consistent with the granite being stiffer than the surrounding rocks. However, a number of the other wells (Moomba-73, Moomba-78, Big Lake-54 and Bulyeroo-1), which are also close to the granite bodies, exhibit an east–west S_{Hmax} stress orientation and appear unperturbed by the granite bodies. It should be noted that the effect of the granite body at Moomba-73 could not be assessed, as the regional east–west S_{Hmax} orientation is perpendicular to the granite body. Because the other wells close to the granite bodies are unperturbed, we feel the stress rotation in Cowan-3 is probably a result of an unidentified fault or local variations in the rock elastic properties not yet identified.

7 CONCLUSIONS

Borehole breakouts and DITFs from 61 wells in the Cooper Basin indicate an average S_{Hmax} orientation of 101°N (A–C quality data). A total of 890 borehole breakouts and 608 DITFs were interpreted in the Cooper Basin. The average S_{Hmax} orientation is consistent between different data types and different data quality. The mean east–west S_{Hmax} orientation determined for the Cooper Basin is orthogonal to the direction of absolute plate velocity for the IAP. Within the Cooper Basin a significant stress rotation occurs from the east–west S_{Hmax} orientation in the Nappamerri Trough, and much of the basin, to northwest–southeast S_{Hmax} orientation in the Patchawarra Trough. This rotation is part of a larger scale horseshoe-shaped stress rotation across central eastern Australia between the Amadeus, Cooper and Bowen basins.

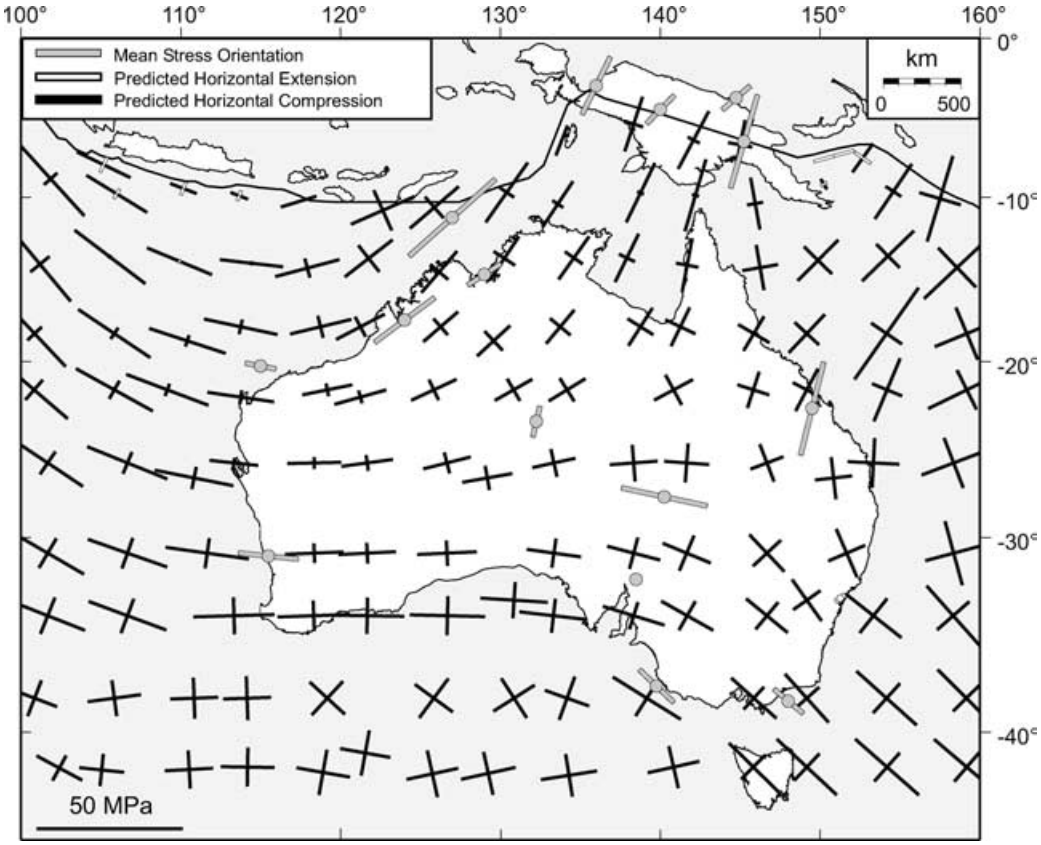

Figure 8. Best-fitting plate boundary force model displaying the predicted stresses across continental Australia from Reynolds *et al.* (2002). The predicted stress orientations were constrained using all 12 stress provinces (including the Cooper Basin) defined in Reynolds *et al.* (2002).

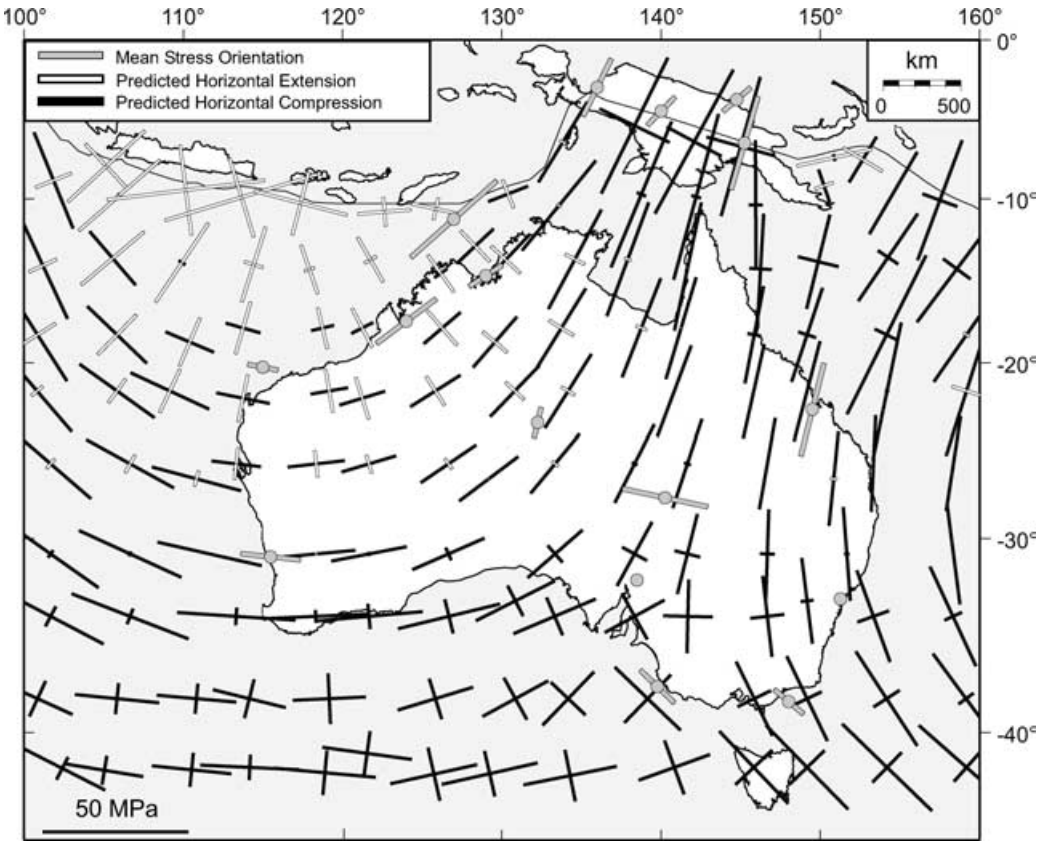

Figure 9. Best-fitting plate boundary force model determined when excluding the east–west S_{Hmax} orientation in the Cooper Basin to constrain the model.

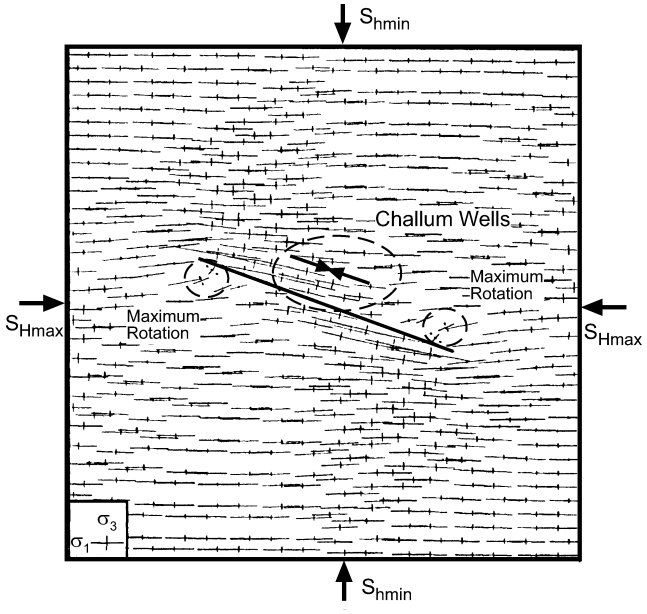

Figure 10. Predicted stress rotation around a single discontinuity showing fault parallel S_{Hmax} orientations along the mid-section of the fault (adapted from Homberg *et al.* 1997). The average stress S_{Hmax} orientation from the three Challum wells has been superimposed on the modelled stress field. Model uses a differential stress ($S_{Hmax} - S_{hmin}$) of 50 MPa and 20° angle between fault strike and the S_{Hmax} orientation. Model results are applicable to strike-slip deformation, which is consistent with the stress magnitude estimates in the Cooper Basin suggesting a strike-slip faulting stress regime (Hillis *et al.* 1998).

Finite element modelling of the *in situ* stress field of the IAP using a range of plate-scale tectonic forces is able to match the S_{Hmax} orientation over most of Australia reasonably well, including the mean east–west S_{Hmax} orientation in the Cooper Basin. However, plate boundary–scale modelling cannot adequately match the horseshoe-shaped stress rotation between the Amadeus, Cooper and Bowen basins. A large combination of plate boundary forces can be used to match the mean east–west S_{Hmax} orientation in the Cooper Basin. Nonetheless, the Cooper Basin stress field suggests that stresses from tensional forces acting along the Tonga–Kermadec subduction zone are not transmitted into the interior of the Australian Plate. More *in situ* stress data are required in the areas to the northeast and northwest of the Cooper Basin in order to improve the plate-scale modelling and further account for the horseshoe-shaped stress rotation. A number of smaller scale stress features have been identified within the *in situ* stress data that cannot be explained by plate-scale tectonic forces. These features are possibly a result of local geological structure and/or density contrasts perturbing the stress field.

ACKNOWLEDGMENTS

The authors wish to thank Santos and their joint venture partners, Delhi Petroleum, Origin Energy, Gulf (Australia) and Basin Oil for providing data and allowing publication of the results. Primary Industries and Resources South Australia is also thanked for providing access to image log data. The depth to basement map for the Cooper Basin was kindly provided by Primary Industries and Resources South Australia, Queensland Department of Mines and Energy, Northern Territory Department of Mines and Energy, Mineral Resources New South Wales and Geoscience Australia. JRS Petroleum Research is thanked for the use of the SWIFT software package. This research has been part of the Australasian Stress Map project funded by an Australian Research Council grant. Dietmar Müller and two anonymous reviewers are thanked for their comments.

REFERENCES

Aleksandroski, P., Inderhaug, O.H. & Knapstad, B., 1992. Tectonic structures and wellbore breakout orientation. In: *33rd US Symposium on Rock Mechanics, Santa Fe,* pp. 29–37, eds Tillerson, J.R. & Wawersik, W., A.A. Balkema Publishers, Rotterdam, the Netherlands.

Apak, S.N., Stuart, W.J., Lemon, N.M. & Wood, G., 1997. Structural evoluation of the Permian-Triassic Cooper Basin, Australia: Relation to hydrocarbon trap styles, *AAPG Bull.,* **81,** 533–555.

Assameur, D.M. & Mareschal, J.-C., 1995. Stress induced by topography and crustal density heterogeneities: Implications for the seismicity of southeastern Canada, *Tectonophysics,* **241,** 179–192.

Barton, C.A., Castillo, D.A., Moos, D., Peska, P. & Zoback, M.D., 1998. Characterising the full stress tensor based on observations of drilling-induced wellbore failures in vertical and inclined boreholes leading to improved wellbore stability and permeability prediction, *APPEA J.,* **38,** 466–487.

Bell, J.S., 1996. Petro Geoscience 2, in situ stresses in sedimentary rocks (part 2): applications of stress measurements, *Geoscience Canada,* **23,** 135–153.

Bell, J.S. & Gough, D.I., 1979. Northeast-southwest compressive stress in Alberta - evidence from oil wells, *Earth planet. Sci. Lett.,* **45,** 475–482.

Bird, P., 2003. An updated digital model of plate boundaries, *Geochem. Geophys. Geosyst.,* **4,** doi:10.1029/2001GC000252.

Brudy, M. & Zoback, M.D., 1999. Drilling-induced tensile wall-fractures: implications for determination of in-situ stress orientation and magnitude, *Int. J. Rock Mech. Min. Sci.,* **36,** 191–215.

Cloetingh, S. & Wortel, R., 1986. Stress in the Indo-Australia plate, *Tectonophysics,* **132,** 49–67.

Coblentz, D.D., Sandiford, M., Richardson, R.M., Zhou, S. & Hillis, R.R., 1995. The origins of the intraplate stress field in continental Australia, *Earth planet. Sci. Lett.,* **133,** 299–309.

Coblentz, D.D., Zhou, S., Hillis, R.R., Richardson, R.M. & Sandiford, M., 1998. Topography, boundary forces, and the Indo–Australian intraplate stress field, *J. geophys. Res.,* **103,** 919–931.

Dart, C.J., Inderhaug, O.H., Klovjan, O. & Ottesen, C., 1995. The present day stress regime in the Barents sea from borehole breakout. In: *Workshop on Rock Stresses in the North Sea, Trondheim, Norway,* pp. 179–190, eds Fejerskov, M. & Myrvang, A.M.

Dyksterhuis, S. & Müller, R.D., 2004. Modelling the contemporary stress field of the Australian contient, *Preview,* **109,** 26–29.

Gatehouse, C.G., Fanning, C.M. & Flint, R.B., 1995. Geochronology of the Big Lake Suite, Warburton Basin, northeastern South Australia, *South Australia Geological Survey Quarterly Geological Notes,* **128,** 8–16.

Gölke, M. & Coblentz, D., 1996. Origins of the European regional stress field, *Tectonophysics,* **266,** 11–24.

Gough, D.I. & Bell, J.S., 1982. Stress orientations from borehole wall fractures with examples from Colorado, east Texas, and northern Canada, *Can. J. Earth Sci.,* **19,** 1358–1370.

Gravestock, D.I. & Jensen-Schmidt, B., 1998. Structural Setting, in, *Petroleum Geology of South Australia: Cooper Basin,* Vol. 4, pp. 47–67, eds Gravestock, D.I., Hibburt, J.E. & Drexel, J.F., Department of Primary Industries and Resources SA, Adelaide, Australia.

Hansen, K.M. & Mount, V.S., 1990. Smoothing and extrapolation of crustal stress orientation measurements, *J. geophys. Res.,* **95,** 1155–1165.

Hill, A.J. & Gravestock, D.I., 1995. Cooper Basin, in *The Geology of South Australia: The Phanerozoic* Vol. 2, pp. 78–87, eds Drexel, J.F. & Preiss, W.V., South Australia Geological Survey, Bulletins54.

Hillis, R.R., Meyer, J.J. & Reynolds, S.D., 1998. The Australian stress map, *Exploration Geophysics,* **29,** 420–427.

Hillis, R.R., Enever, J.R. & Reynolds, S.D., 1999. in situ field of eastern Australia, *Aust. J. Earth Sci.,* **46,** 813–825.

Hillis, R.R. & Reynolds, S.D., 2000. The Australian Stress Map, *J. geol. Soc. Lond.,* **157,** 915–921.

Homberg, C., Hu, J.C., Angelier, J., Bergerat, F. & Lacombe, O., 1997. Characterization of stress pertubations near fault zones: insights from 2-D distinct-element numerical modelling and field studies (Jura mountains), *Journal of Structural Geology,* **19,** 703–718.

Homberg, C., Angelier, J., Bergerat, F. & Lacombe, O., 2004. Using stress deflections to identify slip events in fault systems, *Earth planet. Sci. Lett.,* **217,** 409–424.

Laws, R.A. & Gravestock, D.I., 1998. Introduction, in, *Petroleum Geology of South Australia: Cooper Basin,* Vol. 4, pp. 1–6, eds Gravestock, D.I., Hibburt, J.E. & Drexel, J.F., Department of Primary Industries and Resources SA, Adelaide, Australia.

Mandal, P., Manglik, A. & Singh, R.N., 1997. Intraplate stress distribution induced by topography and crustal density heterogeneities beneath the Killari, India, region, *J. geophys. Res.,* **102,** 11 719–11 729.

Mareschal, J.C. & Kuang, J., 1986. Intraplate stresses and seismicity: the role of topography and density heterogeneities, *Tectonophysics,* **132,** 153–162.

Peska, P. & Zoback, M.D., 1995. Compressive and tensile failure of inclined well bores and determination of in situ and rock strength, *J. Geophys. Res.,* **100,** 12 791–12 811.

Reynolds, S.D. & Hillis, R.R., 2000. The in situ stress field of the Perth Basin, Australia, *Geophys. Res. Lett.,* **27,** 3421–3424.

Reynolds, S.D., Coblentz, D.D. & Hillis, R.R., 2002. Tectonic forces controlling the regional intraplate stress field in continental Australia: results from new finite-element modelling, *J. geophys. Res.,* **107,** 10.1029/2001JB000408.

Richardson, R.M., 1992. Ridge forces, absolute plate motions, and the intraplate stress field, *J. geophys. Res.,* **97,** 11 739–11 748.

Yale, D.P., Rodriguez, J.M. & Mercer, T.B., 1994. In-situ stress orientation and the effects of local structure—Scott Field, North Sea. In: *Eurock '94,* pp. 945–952, A.A. Balkema Publishers, Rotterdam, the Netherlands.

Zellmer, K.E. & Taylor, B., 2001. A three-plate kinematic model for Lau Basin opening, *Geochem. Geophys. Geosyst.,* **2,** doi: 10.1029/2000GC000106.

Zhang, Y.-Z., Dusseault, M.B. & Yassir, N.A., 1994. Effects of rock anisotropy and heterogeneity on stress distributions at selected sites in North America, *Econ. Geol.,* **37,** 181–197.

Zoback, M.L., 1992. First- and second-order patterns of stress in the lithosphere: The world stress map project, *J. geophys. Res.,* **97,** 11 703–11 728.

Zoback, M.D., Moos, D., Mastin, L. & Anderson, R.N., 1985. Well bore breakouts and in situ stress, *J. geophys. Res.,* **90,** 5523–5530.

Zoback, M.L. *et al*., 1989. Global patterns of tectonic stress, *Nature,* **341,** 291–298.